34th Annual International Conference of the IEEE EMBS
San Diego, California USA, 28 August - 1 September, 2012

Quantifying uncertainty in Transcranial Magnetic Stimulation – a high resolution simulation study in ICBM space

Nicola Toschi, Martin E. Keck, Tobias Welt, and Maria Guerrisi

Abstract— **Transcranial Magnetic Stimulation offers enormous potential for noninvasive brain stimulation. While it is known that brain tissue significantly "reshapes" induced field and charge distributions, most modeling investigations to-date have focused on single-subject data with limited generality. Further, the effects of the significant uncertainties which exist in the simulation (i.e. brain conductivity distributions) and stimulation (e.g. coil positioning and orientations) setup have not been quantified. In this study, we construct a high-resolution anisotropic head model in standard ICBM space, which can be used as a population-representative standard for bioelectromagnetic simulations. Further, we employ Monte-Carlo simulations in order to quantify how uncertainties in conductivity values propagate all the way to induced field and currents, demonstrating significant, regionally dependent dispersions in values which are commonly assumed "ground truth". This framework can be leveraged in order to quantify the effect of any type of uncertainty in noninvasive brain stimulation and bears relevance in all applications of TMS, both investigative and therapeutic.**

I. Introduction

A. Transcranial Magnetic Stimulation: pitfalls, potential and models

Transcranial magnetic stimulation (TMS) employs time-varying electromagnetic fields to induce fields/currents within brain tissue, allowing selective, non-invasive and painless interference with brain function. TMS is being increasingly used in neuroscience research and as a therapeutic tool in neurology, psychiatry and rehabilitation [1]. It has long been recognized that the size, shape and distribution of brain tissue have a significant influence on the conductive phenomena ultimately elicited by TMS, and finite-element-based approaches have been employed in order to study how induced fields are shaped by cortical geometry [2], tissue type and anisotropy [3], while finite-difference based algorithms have proven useful in elucidating the departure from the presumed focality in figure-8 stimulation and the clinical relevance of slight variations in coil positioning [4]. However, to our knowledge, studies to date have constructed models based on single subject imaging data, limiting the generality of results precisely because of the high degree of dependence of TMS outcome on local, individual tissue geometry.

N.Toschi and M Guerrisi are with the Medical Phsyics Section, Faculty of Medicine, University of Rome "Tor Vergata" (corresponding author: NT, phone: +39-06-72596008; e-mail: toschi@ med.uniroma2.it). M.E. Keck is with the Center of Neuroscience Research Zurich (ZNZ) and Privatklinik Schlössli, Oetwil am See/Zurich, Switzerland. T. Welt is with the Psychiatrische Universitätsklinik Zürich, Zurich, Switzerland.

B. Brain tissue conductivity estimation – procedures and uncertainties

The lack of extensive in-vivo conductivity measurements leads to an uncertainty in commonly adopted values which is usually estimated around 10% [5]. Also, it is well known that the conductivity of brain tissue is anisotropic at least in white matter. A linear relationship between the apparent water self-diffusion tensor (as measured by Diffusion-Tensor Imaging - DTI) and the conductivity tensor has been proposed [6], which relates the two transport tensors through a perturbation expansion in the statistical correlations of the microstructure. However, the estimates in the linear regression coefficients carry an uncertainty of over 5%, and concerns were raised about the validity of this linear relationship in an in-vitro study performed on excised brain tissue in patients undergoing neurosurgery [7]. Lastly, it should be noted that diffusion weighted images are significantly corrupted by Rician-distributed or non-central Chi-distributed noise which inevitably propagates to conductivity tensor estimation.

C. Aims of the study

The aims of this study are therefore twofold: 1) Establishing an accurate modelling framework in which bioelectromagnetic problems can be solved over a model of the human head derived from a high number of subjects in standard space, and 2) Quantifying the propagation of the cumulative uncertainties which corrupt conductivity tensor estimation through extensive Monte-Carlo simulations which leverage the previously established framework.

II. Materials and Methods

A. Construction of anisotropic conductivity head model in International Consortium for Brain Mapping (ICBM) space

Isotropic tissue conductivity distribution was derived from the MNI (Montreal Neurological Institute) ICBM152 template at 1x1x1 mm^3 resolution, which is an average of 152 subjects (MNI152, available as part of part of FSL 4.1.9 [8]). The MNI152 template was segmented based on a hidden Markov random field model and an associated Expectation-Maximization algorithm using FAST (FMRIB's Automated Segmentation Tool), also part of FSL (Fig. 1). Remaining soft tissue masks were generated by subtraction, and segmentation masks were used to assign isotropic conductivity values (skull: 0.0042, whiter matter: 0.126, grey matter: 0.337, skin and soft tissue: 0.33, CSF: 1.79, all

values in S/m) as previously described [4]. The resulting isotropic conductivity map is shown in Fig. 2.

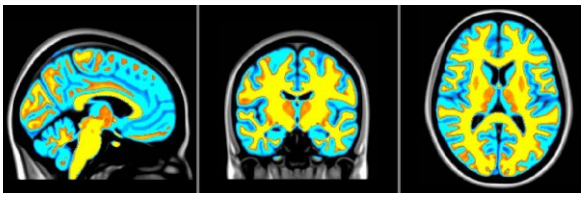

Fig. 1: initial segmentation result. Blue: gray matter. Red-Yellow: white matter. The MN152 T1 template is overlayed for reference.

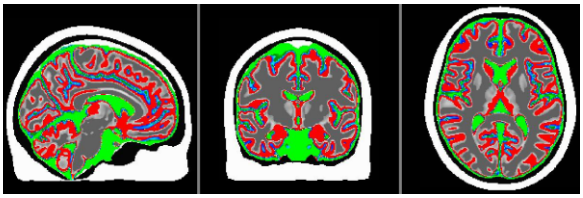

Fig. 2: initial isotropic conductivity head model in MNI152 space. Values range from 0 S/m (air, black) to 1.67 S/m (CSF, green).

The inclusion of an anisotropic conductivity tensor model employed an enhanced diffusion tensor template (IIT2 template, [9]) obtained from 67 subjects and accurately coregistered into MNI152 space. The IIT2 template was mapped into an estimate of the conductivity tensor using the volume constraint method, which involves solving the following equations for each voxel:

$$\frac{s_1}{\lambda_1} = \frac{s_2}{\lambda_2} = \frac{s_3}{\lambda_3}; \quad \sqrt[3]{s_1 s_2 s_3} = s_{iso} \tag{1}$$

where λ_i is the *i*th diffusion tensor eigenvalue, s_i is the *i*th conductivity tensor eigenvalue, and s_{iso} is the isotropic conductivity value assigned to each voxel in the previous step.

B. Solution of the Electromagnetic Problem

As previously shown [4], in the quasi-static limit the system is governed by the following:

$$\begin{aligned} &\nabla \cdot \left(\mathbf{C} \cdot \nabla \Phi\right) = -\nabla \cdot \left(\mathbf{C} \cdot \frac{\partial \mathbf{A}}{\partial t}\right) \\ &\mathbf{n} \cdot \mathbf{J} = 0 \\ &\mathbf{J} = \mathbf{C} \cdot \mathbf{E} \end{aligned} \tag{2}$$

where Φ is the scalar electrostatic potential, $\mathbf{E}$ is total electric field, $\mathbf{n}$ is normal to the outer bounding surface, and $\mathbf{C}$ is the electrical conductivity tensor. In the quasi-static limit, the magnetic vector potential $\mathbf{A}$ is due only to the current density $\mathbf{J}_{coil}$ flowing in the induction coil and can be evaluated preventively as:

$$\mathbf{A} = p(t)\frac{\mu}{4\pi}\int \frac{\mathbf{J}_{coil}}{|\mathbf{r} - \mathbf{r}'|} d^3\mathbf{r}' = p(t)\mathbf{A}'(\mathbf{r}) \tag{3}$$

where p(t) is the time-dependent component of $\mathbf{A}$, μ is the total magnetic permeability of tissue (very close to unity) and is $\mathbf{r}$ the position vector. The simulated stimulation setup employed a standard "figure-8" coil (MC-B70, 2x10 windings, inner radius: 10 mm, outer radius: 50 mm, winding height 6mm) which was placed symmetrically and horizontally over the model head. Eqn. (3) was solved numerically using a systematic over-relaxation method based on a finite-difference stencil capable of accounting for anisotropic conductivity through an *ad hoc* developed FORTRAN 90 implementation.

C. Monte Carlo Simulations: Perturbation of tensor size and orientations

In order to investigate how uncontrolled perturbations in conductivity values can affect the resulting estimates of conductive phenomena of tissue, we perturbed both tensor size and orientation as follows:

$$\begin{aligned} &\mathbf{C}^{s,o} = \mathbf{R}^T \mathbf{C}\left(1 + \mathrm{N}\left(0, \sigma_{shape}\right)\right)\mathbf{R}; \\ &\mathbf{R} = \mathbf{R}(\alpha, \beta, \gamma); \quad \alpha, \beta, \gamma = \mathrm{N}\left(0, \sigma_{orient}\right) \end{aligned} \tag{4}$$

where $\mathbf{C}^{s,o}$ and $\mathbf{C}$ are the perturbed and unperturbed conductivity tensor distribution over the whole head, respectively. The standard deviation (s.d.) σ_{shape} was 0.05. A random rotation $\mathbf{R}$ was also applied to each tensor, characterised by randomly sampled Euler angles (α, β, γ) distributed around mean 0 with a s.d. of 4 degrees. 200 realisations of the conductivity tensor field were generated for subsequent repeated solution of the EM problem.

D. Quantification of perturbation of induced fields and currents

For each realisation, we computed the scalar quantity Φ, the vectorial quantities $\mathbf{E}$, $\mathbf{J}$ and their respective scalar moduli. Voxel-based means and standard deviation were computed for scalar quantities. For vectorial quantities, the uncertainty in orientation was quantified by computing the dyadic coherence and the cone of uncertainty. Specifically, for a unit length vector $\mathbf{v}$, the mean dyadic tensor was calculated as:

$$\left\langle \mathbf{v}^j \cdot \mathbf{v}^{j\mathrm{T}} \right\rangle = \left\langle \begin{vmatrix} \left(\mathbf{v}_x^j\right)^2 & \mathbf{v}_x^j \mathbf{v}_y^j & \mathbf{v}_x^j \mathbf{v}_z^j \\ \mathbf{v}_x^j \mathbf{v}_y^j & \left(\mathbf{v}_y^j\right)^2 & \mathbf{v}_y^j \mathbf{v}_z^j \\ \mathbf{v}_x^j \mathbf{v}_z^j & \mathbf{v}_y^j \mathbf{v}_z^j & \left(\mathbf{v}_z^j\right)^2 \end{vmatrix} \right\rangle = \frac{1}{100}\sum_{j=1}^{100} \mathbf{v}^j \cdot \mathbf{v}^{j\mathrm{T}} \tag{5}$$

where $\mathbf{v}_i^j$ is the *i*th component of the *j*th realisation of $\mathbf{v}$. Each individual dyadic tensor has only one non-zero eigenvalue and a principal eigenvector which is parallel to the vector from which the dyad is formed, while the average dyad (mean dyadic tensor) has eigenvectors $\mathbf{\Psi}_i$ and eigenvalues β_i. The dyadic coherence κ of the 100 realizations is then defined as $\kappa = \left(1 - \sqrt{(\beta_2 + \beta_3)/2\beta_1}\right)$ and takes values from zero (when all the $\mathbf{v}^j$ are uniformly distributed over the unit sphere), to one when all $\mathbf{v}^j$ are

collinear. Further, the angle subtended between each realisation $\mathbf{v}^j$ and the average principal eigenvector $\mathbf{\Psi}_1$ was calculated as $\theta^j = \text{acos}\left(\mathbf{v}^j \cdot \mathbf{\Psi}_1\right)$, and 95% confidence intervals for θ (which define the cone of uncertainty) were computed in each voxel using the percentile method. This procedure was applied to the unit length-vectors $\mathbf{E}/|\mathbf{E}|$ and $\mathbf{J}/|\mathbf{J}|$.

III. Results

The first result of the above procedure is a full, anisotropic model of the conductivity distribution of the human head in MNI152 space which is employed in all subsequent simulations (Fig. 3).

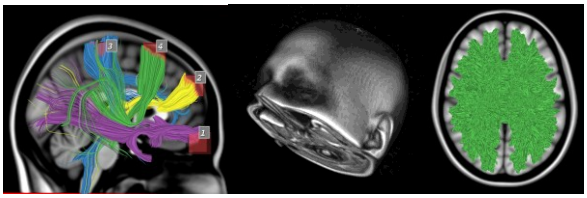

Fig. 3: 3D- rendering of MNI152 template used for tissue segmentation (middle); example fiber tracts reconstructed from the IIT2 template and overlayed on the MNI152 template (left). Full set of fibers reconstructed and used in conductivity tensor estimation (right).

A. Quantification of current density induced in the "standard" ICBM brain and effects of anisotropy

Fig. 4 show a sample simulation result which summarises the primary field as well as the total currents induced in the head model.

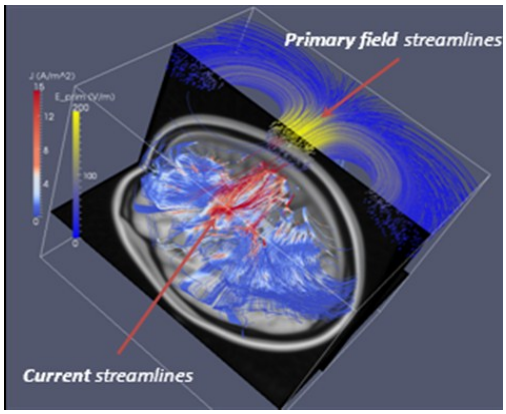

Fig. 4: Sample simulation results. 3D rendering of primary field streamlines (blue - yellow) and total current streamlines (red-blue).

The induced currents show a significant departure from the regular spatial arrangement of the primary field. Also, the inclusion of conductivity anisotropy in the model affords significant corrections in the resulting induced currents. Fig. 5 shows a comparison of identical simulations run with an isotropic and anisotropic model, respectively (i.e. the conductivity tensor in Eqn. 2 was substituted with a diagonal tensor with trace $3s_{iso}$).

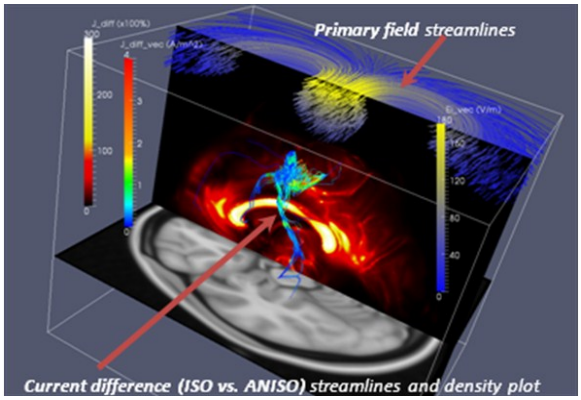

Fig. 5: Comparison of simulation results obtained using isotropic and anisotropic head models. 3D rendering of primary field streamlines (blue - yellow), streamlines of the algebraic difference between the current density $\mathbf{J}_{iso}$ (obtained using the isotropic model) and $\mathbf{J}_{aniso}$ (obtained using the anisotropic model). The difference is also rendered as a density plot in the sagittal section (black-red).

B. Dispersion of moduli and orientations of induced field and currents

The bootstrap/Monte Carlo procedure results in spatial uncertainty maps in $\mathbf{J}$ and $\mathbf{E}$ in terms of both magnitude (relative errors, Figures 6 and 8, respectively) and orientation (coherence and confidence intervals, Figure 10).

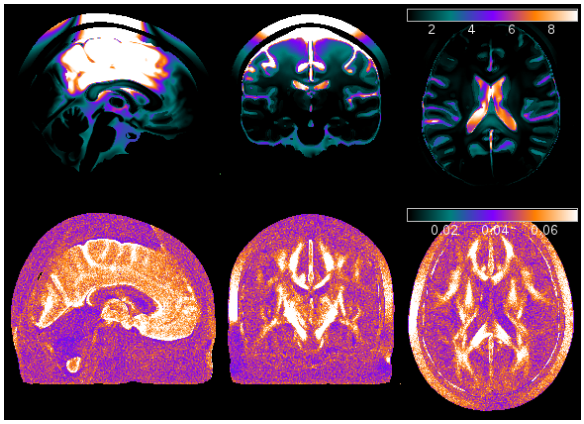

Fig. 6: Mean (top, A/m^2) and relative error (s.d./mean, unitless) of $|\mathbf{J}|$

The uncertainty distributions of $\mathbf{J}$ and $\mathbf{E}$ can be also visualized as a function of Fractional Anisotropy (FA – normalized variance of eigenvalues) or tensor Trace (sum of eigenvalues) in order the evaluate the dependence of uncertainty on tissue configuration. Figures 7 and 9 provide an example of this visualization.

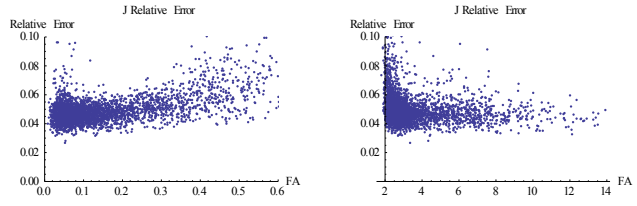

Fig. 7: Whole-brain scatterplot of relative error (s.d./mean, unitless) of $|\mathbf{J}|$ as a function of Fractional Anisotropy (FA - left) and Tensor Trace (right)

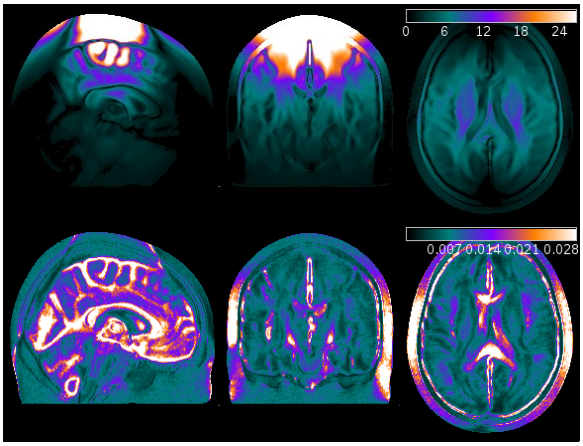

Fig. 8: Mean (top, V/m) nd relative error (s.d./mean, unitless) of $|\mathbf{E}|$

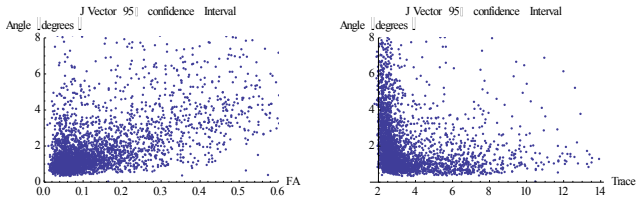

Fig. 9: Whole-brain scatterplot of 95% confidence interval (degrees) of **J** orientation as a function of Fractional Anisotropy (FA -left) and Tensor Trace (right).

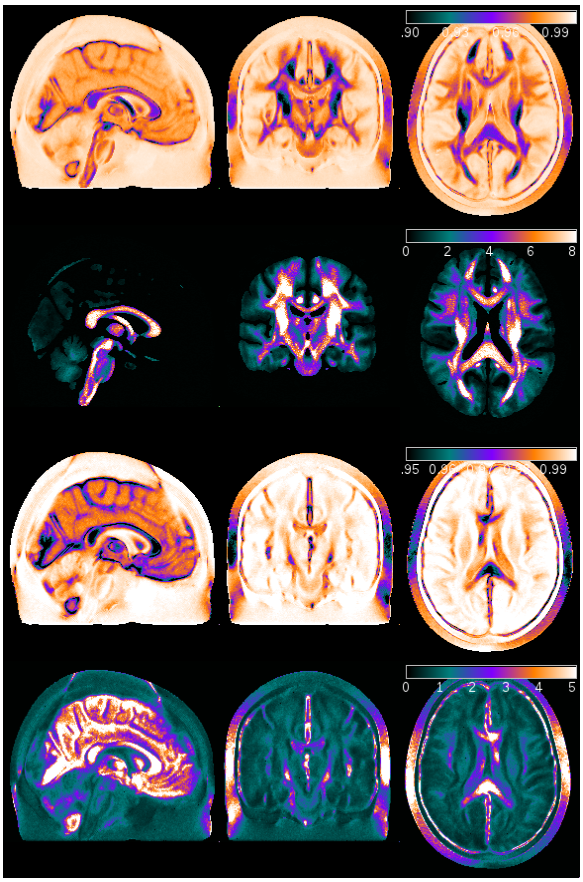

Fig. 10: dyadic coherence and 95% confidence interval (bottom) of **J** (top two panes) and **E** (two bottom panes)

IV. Discussion and Conclusions

Compared to other high-resolution models, the model built in this study is based on templates which are representative of hundreds of subjects and is hence can be employed to test simulated novel setups, EEG source localisation techniques, or the effects of conductivity or coil positioning perturbation without the restriction of working in one particular subject's space. This is particularly relevant in view of the growing body of literature which has highlighted the sensitivity of TMS outcome on inter-individual anatomical variability. Conversely, our Monte-Carlo methodology can be employed in single-subject space if needed. As an example application, we have demonstrated (Figures 6-10) how the uncertainty associated with head conductivity estimation propagates in a markedly inhomogeneous manner, which is also highly dependent on anatomy. For example, for a given perturbation in conductivity, a larger loss of directional coherence (up to 8-9 degrees confidence interval) in induced current density is observed in white matter (high FA and low trace) areas when compared to gray matter, while current density magnitude shows a slight tendency in the opposite directions. Such results exemplify how our framework can be expanded to quantify the sensitivity of uncertainties in all TMS variables in a regional manner, eventually providing a quantitative guide to interpreting the variability in outcome of stimulation when a specific area is targeted in terms of the perturbational "sensitivity" of that particular area.

References

[1] T. Wagner, A. Valero-Cabre, and A. Pascual-Leone, "Noninvasive human brain stimulation," *Annu Rev Biomed Eng,* vol. 9, pp. 527-65, 2007.

[2] A. Thielscher, A. Opitz, and M. Windhoff, "Impact of the gyral geometry on the electric field induced by transcranial magnetic stimulation," *Neuroimage,* vol. 54, pp. 234-43, Jan 1 2011.

[3] A. Opitz, M. Windhoff, R. M. Heidemann, R. Turner, and A. Thielscher, "How the brain tissue shapes the electric field induced by transcranial magnetic stimulation," *Neuroimage,* vol. 58, pp. 849-59, Oct 1 2011.

[4] N. Toschi, T. Welt, M. Guerrisi, and M. E. Keck, "Transcranial magnetic stimulation in heterogeneous brain tissue: clinical impact on focality, reproducibility and true sham stimulation," *J Psychiatr Res,* vol. 43, pp. 255-64, Jan 2009.

[5] T. A. Wagner, M. Zahn, A. J. Grodzinsky, and A. Pascual-Leone, "Three-dimensional head model simulation of transcranial magnetic stimulation," *IEEE Trans Biomed Eng,* vol. 51, pp. 1586-98, Sep 2004.

[6] D. S. Tuch, V. J. Wedeen, A. M. Dale, J. S. George, and J. W. Belliveau, "Conductivity tensor mapping of the human brain using diffusion tensor MRI," *Proc Natl Acad Sci U S A,* vol. 98, pp. 11697-701, Sep 25 2001.

[7] M. Akhtari, N. Salamon, R. Duncan, I. Fried, and G. W. Mathern, "Electrical conductivities of the freshly excised cerebral cortex in epilepsy surgery patients; Correlation with pathology, seizure duration, and diffusion tensor imaging," *Brain Topogr,* vol. 18, pp. 281-290, Sum 2006.

[8] S.M. Smith et al, Advances in functional and structural MR image analysis and implementation as FSL," *NeuroImage*, vol, 23(S1), pp 208-219, 2004.

[9] S. Zhang, H. Peng, R. J. Dawe, and K. Arfanakis, "Enhanced ICBM diffusion tensor template of the human brain," *Neuroimage,* vol. 54, pp. 974-84, Jan 15 2011.